

Theoretical search for possible Li–Ni–B crystal structures using an adaptive genetic algorithm ^F

Cite as: J. Appl. Phys. **127**, 094902 (2020); <https://doi.org/10.1063/1.5138642>

Submitted: 19 November 2019 . Accepted: 15 February 2020 . Published Online: 02 March 2020

Renhai Wang ^{id}, Yang Sun ^{id}, Volodymyr Gvozdetzkyi ^{id}, Xin Zhao, Feng Zhang, Lin-Han Xu, Julia V. Zaikina, Zijing Lin, Cai-Zhuang Wang, and Kai-Ming Ho

COLLECTIONS

^F This paper was selected as Featured



View Online



Export Citation



CrossMark

ARTICLES YOU MAY BE INTERESTED IN

Regenerative cooling using elastocaloric rubber: Analytical model and experiments

Journal of Applied Physics **127**, 094903 (2020); <https://doi.org/10.1063/1.5132361>

Dynamic experiments to study the α – ϵ phase transition in cerium

Journal of Applied Physics **127**, 095901 (2020); <https://doi.org/10.1063/1.5142508>

An efficient wideband cross-polarization converter manufactured by stacking metal/dielectric multilayers via 3D printing

Journal of Applied Physics **127**, 093103 (2020); <https://doi.org/10.1063/1.5135632>

Lock-in Amplifiers
Find out more today



Zurich
Instruments






Theoretical search for possible Li-Ni-B crystal structures using an adaptive genetic algorithm

Cite as: J. Appl. Phys. **127**, 094902 (2020); doi: [10.1063/1.5138642](https://doi.org/10.1063/1.5138642)

Submitted: 19 November 2019 · Accepted: 15 February 2020 ·

Published Online: 2 March 2020



Renhai Wang,^{1,2}  Yang Sun,²  Volodymyr Gvozdetzkyi,³  Xin Zhao,² Feng Zhang,² Lin-Han Xu,⁴ Julia V. Zaikina,³ Zijing Lin,^{1,a)} Cai-Zhuang Wang,² and Kai-Ming Ho^{2,5,a)}

AFFILIATIONS

¹Department of Physics, University of Science and Technology of China, Hefei 230026, China

²Ames Laboratory, U.S. DOE and Department of Physics, Iowa State University, Ames, Iowa 50011, USA

³Department of Chemistry, Iowa State University, Ames, Iowa 50011, USA

⁴Department of Physics, Xiamen University, Xiamen 361005, China

⁵International Center for Quantum Design of Functional Materials (ICQD), Hefei National Laboratory for Physics Sciences at the Microscale, University of Science and Technology of China, Hefei 230026, China

^{a)}Authors to whom correspondence should be addressed: kmh@iastate.edu and zjlin@ustc.edu.cn

ABSTRACT

The structural diversity of rare-earth and transition metal borides indicates that alkali-transition metal borides (*A-T-B*) show tremendous promise in exhibiting a variety of crystal structures with different dimensionalities of *T-B* frameworks. On the other hand, the *A-T-B* ternary systems are severely underexplored because of the synthetic challenges associated with their preparation. Accurate and efficient computational predictions of low-energy stable and metastable phases can identify the optimal compositions of the hypothetical compounds in the *A-T-B* systems to guide the synthesis. In this work, we have computationally discovered several new phases in the Li-Ni-B ternary system. The newly discovered LiNiB, Li₂Ni₃B, and Li₂NiB phases expand the existing theoretical database, and the convex-hull surface of Li-Ni-B has been re-constructed. The lowest energy structure of the LiNiB compound has been found by an adaptive genetic algorithm with layered motif, which matches with the experimentally determined structure. According to our electrochemical calculations, LiNiB and another predicted layered Li₂NiB compounds have great potential as anode materials for lithium batteries. The Li₂Ni₃B compound with the space group *P*4₃32 was predicted to crystallize in a cubic structure composed of distorted octahedral units of BNi₆, which is isostructural to two noncentrosymmetric superconductors Li₂Pd₃B and Li₂Pt₃B. While we were unable to experimentally confirm the Li₂Ni₃B compound utilizing the hydride synthetic route, attempts to synthesize this compound by alternate methods remain highly desirable, considering its potential superconducting properties.

Published under license by AIP Publishing. <https://doi.org/10.1063/1.5138642>

I. INTRODUCTION

Discovery of new emerging materials can be accelerated if the appropriate experimental methods are combined with high-throughput computations. A combination of both the approaches allows for a more efficient screening of target phases to reduce the vast compositional space in multicomponent systems.^{1,2} With the increased availability of high-power computational resources, a number of different approaches for the prediction of new stable compounds, e.g., simulated annealing,³ random structure searching,⁴ evolutionary algorithms,⁵ particle swarm optimization,^{6,7} have been rapidly developed during the last decade. As a result, numerous

computational material depositories have been founded, including, for example, Materials Project,⁸ Open Quantum Materials Database,⁹ Computational Materials Repository,¹⁰ AFLOW library,¹¹ and Electronic Structure Project.¹² Despite the enormous number of compounds that have been generated theoretically ($\sim 10^4$ – 10^6 entries), these databases only provide limited guidance² for experimentalists to perform targeted screening of new compounds. In certain cases, actual validation and verification of the computational approaches would greatly advance the current knowledge of available compounds for novel synthesis methods.

Borides represent a broad class¹³ of compounds with a variety of structures and properties. The strongest permanent magnet

$\text{Nd}_2\text{Fe}_{14}\text{B}$,¹⁴ magnetocaloric material AlFe_2B_2 ,¹⁵ superconductor below 39 K MgB_2 ,¹⁶ hydrogen evolution catalyst Mo_2B_4 ,¹⁷ super-hard ReB_2 , WB_4 ¹⁸ are examples of functional materials based on borides. The experimental search guided by theoretical predictions provides a great opportunity for the discovery of new borides with diverse structures and potentially interesting properties. Among the ternary borides, borides containing alkali metals and 3d-transition metals deserve particular attention, since only three ternary phases, all of them in the Li–Ni–B system,^{19–23} have been previously reported for 35 A–T–B ternary systems (A = alkali metal, Li, Na, K, Rb, and Cs; T = first-row 3d-transition metal, Ti–Ni). This lack in compounds becomes more apparent when compared to the rare-earth transition metal borides (RE–T–B), where over 450 ternary phases have been reported.²⁴

Given the extraordinary properties of borides, it would be beneficial to develop theoretical methods that could open up their compositional phase space to guide experimental synthesis. Analysis of the structures of ternary RE–T–B indicates the tremendous diversity ranging from layered (2D) to framework-like (3D) structures. There are examples of isostructural A–T–B and RE–T–B compounds, in which the rare-earth and alkali metals are in the same environment. One example is provided by $\text{Li}_3\text{Ni}_{20}\text{B}_6$ [Fig. 1(a)], which is one of the known borides of the three alkali metal and 3d transition metal borides, and the isostructural lutetium nickel boride $\text{Lu}_2\text{Ni}_{21}\text{B}_6$ [Fig. 1(b)]. The difference in stoichiometry is due to the mixed Li/Ni sites in the lithium containing compound, but the lack of those in the lutetium one. The structural diversity of rare-earth and transition metal borides indicates that the under-researched alkali-transition metal borides have tremendous promise to exhibit a variety of crystal structures with various dimensionalities of T–B frameworks. It would be of great interest if more ternary Li–Ni–B compounds were identified.

In this paper, we applied the adaptive genetic algorithm (AGA) to search for possible stable crystal structures of compounds in the Li–Ni–B system. The ability of AGA has been shown previously by solving the crystal structures of large unit cells^{25,26} with ~140 atoms and predicting new ternary compounds.^{23,27} Our studies not only successfully validated the new experimentally synthesized LiNiB phase²³ but also predicted another two possible phases, $\text{Li}_2\text{Ni}_3\text{B}$ and Li_2NiB . $\text{Li}_2\text{Ni}_3\text{B}$ is isostructural to two non-centrosymmetric superconductors $\text{Li}_2\text{Pd}_3\text{B}$ and $\text{Li}_2\text{Pt}_3\text{B}$. However, experimental validation

was not successful using the hydride route, unlike the LiNiB compound. The dynamical stability and the electronic properties of the new $\text{Li}_2\text{Ni}_3\text{B}$ were also studied by first-principles calculations. For the two layered compounds (LiNiB and Li_2NiB), we explored their potential to become anode materials for lithium batteries by calculating their voltage platforms during the process of lithiation and delithiation. Finally, we updated the theoretical phase diagram of the Li–Ni–B ternary system with our new density functional theory (DFT) calculations. The predictions from our theoretical studies would provide useful guidance for experimental synthesis and discovery of new compounds for Li–Ni–B and similar systems.

II. COMPUTATIONAL METHODS

Crystal structures of Li–Ni–B were investigated by AGA,^{25,28} which integrates auxiliary interatomic potentials (for GA loop) and first-principles calculations (for adaptive loop) together in an adaptive manner to ensure high efficiency and accuracy. The structure searches were only constrained by the chemical composition, without any assumption on the Bravais lattice type, symmetry, atom basis, or unit cell dimensions. In the AGA searches, energy was used as the only criteria for optimizing the candidate pool. The pool size of the candidate structures in GA search is 128. At each GA generation, 32 new structures are generated from the parent structure pool via the mating procedure described in Ref. 29. The structures in the pool were updated by keeping the lowest 128 structures. The structure search with a given auxiliary interatomic potential was carried out for 600 consecutive GA generations. Then, 16 structures were randomly selected from the final pool of the GA search for first-principles calculations to readjust the potential parameters of the auxiliary classical potential for the next round of the GA search. The adaptive process was repeated for 40 iterations.

In the AGA search for the Li–Ni–B system, interatomic potentials based on the embedded-atom method (EAM)³⁰ were chosen as the auxiliary classical potential. In EAM, the total energy of an N-atom system is described by

$$E_{\text{total}} = \frac{1}{2} \sum_{i,j(i \neq j)}^N \phi(r_{ij}) + \sum_i F_i(n_i), \quad (1)$$

where $\phi(r_{ij})$ is the pair interaction between atoms i and j at distance r_{ij} . $F_i(n_i)$ is the embedding term, and the electron density at the site occupied by atom i can be calculated according to $n_i = \sum_{j \neq i} \rho_j(r_{ij})$. The fitting parameters in the EAM formula are chosen as follows: The parameters for Ni–Ni interactions were taken from the literature.³¹ Other pair interactions (Li–Li, B–B, Li–Ni, Li–B, and B–Ni) were modeled by the Morse function

$$\phi(r_{ij}) = D[e^{-2\alpha(r_{ij}-r_0)} - 2e^{-\alpha(r_{ij}-r_0)}], \quad (2)$$

where D , α , r_0 are fitting parameters. The density function for Li and B atoms are modeled by an exponential decaying function

$$\rho(r_{ij}) = \alpha \exp[-\beta(r_{ij} - r_0)], \quad (3)$$

where α and β are fitting parameters. The form proposed by Benerjee and Smith³² was used as the embedding function with

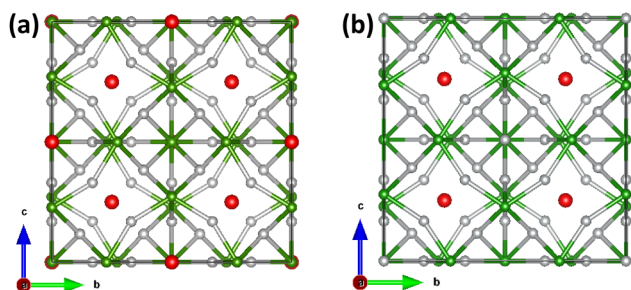


FIG. 1. Crystal structures comparison of A–T–B $\text{Li}_3\text{Ni}_{20}\text{B}_6$ (a) and RE–T–B $\text{Lu}_2\text{Ni}_{21}\text{B}_6$ (b); Li (Lu)–red, Ni–grey, B–green.

fitting parameters F_0 , γ as

$$F(n) = F_0[1 - \gamma \ln n]n^\gamma. \quad (4)$$

For Ni, the parameters of the density function and embedding function were taken from Ref. 31 as well.

According to the AGA scheme,²⁸ the potential parameters were adjusted adaptively by fitting to the DFT energies, forces, and stresses of selected structures. The fitting process was performed by the force-matching method with the stochastic simulated annealing algorithm implemented in the *potfit* code.^{33,34} First-principles calculations were carried out using the projector augmented wave (PAW) method³⁵ within density functional theory (DFT) as implemented in the VASP code.^{36,37} The exchange and correlation energy is treated within the spin-polarized generalized gradient approximation (GGA) and parameterized by the Perdew–Burke–Ernzerhof formula (PBE).³⁸ A plane-wave basis was used with a kinetic energy cutoff of 650 eV. The energy convergence criterion is 10^{-5} eV. The Monkhorst–Pack's sampling scheme³⁹ was adopted for Brillouin zone sampling with a k -point grid of $2\pi \times 0.033 \text{ \AA}^{-1}$, and the ionic relaxations stopped when the forces on every atom became smaller than 0.01 eV/\AA . To characterize the energetic stability of the structures at different compositions obtained from AGA search, the formation energy (E_f) of any given structure $\text{Li}_m\text{Ni}_n\text{B}_p$ was calculated by

$$E_f = \frac{E(\text{Li}_m\text{Ni}_n\text{B}_p) - mE(\text{Li}) - nE(\text{Ni}) - pE(\text{B})}{m + n + p}, \quad (5)$$

where $E(\text{Li}_m\text{Ni}_n\text{B}_p)$ is the total energy of the $\text{Li}_m\text{Ni}_n\text{B}_p$ alloy. $E(\text{Li})$, $E(\text{Ni})$, and $E(\text{B})$ are the per-atom energy of bulk BCC-Li, FCC-Ni, and rhombohedral-B ($R\bar{3}m$), respectively.

III. EXPERIMENTAL SECTION

A. Synthesis

The starting materials for the synthesis were powders of lithium hydride (AlfaAesar, 99.4%), nickel (AlfaAesar, 99.996%), and boron (AlfaAesar, amorphous and crystalline, 98%). All manipulations of the starting materials and samples were performed in an argon-filled glovebox with $p(\text{O}_2) < 1 \text{ ppm}$. Screening of the Li–Ni–B system was done following the typical procedure developed in earlier experimental works.^{22,23} Powders of the starting materials were weighed in LiH: Ni:B = 2:3:1 and 3:3:1 molar ratios and loaded into polystyrene grinding vials set with slip-on caps. The vials were then sealed into a double-sided polypropylene bag under argon atmosphere and brought out for the powder mixing/milling using ball-mill (8000 M MIXER/MILL) for 18 min. Afterward, fine powders were loaded in Ta tubes, which were sealed by arc-melting and placed into silica reactors equipped with Swagelok safety check valves. The reactors were evacuated down to 4×10^{-5} Bar and placed in resistance furnaces (Thermo Scientific Thermolyne Type FD1500 M) connected to thermocontrollers (Eurotherm 3216). Samples were slowly (1.25 K/min) heated from room temperature to 1173 K, held at that temperature for 12 h, and then cooled down to room temperature by switching off the furnace.

B. Powder x-ray diffraction

The phase identification in polycrystalline samples was performed by means of powder x-ray diffraction. Data were collected at room temperature using Rigaku MiniFlex600 powder diffractometer with Cu $K\alpha$ radiation ($\lambda = 1.54051 \text{ \AA}$) and Ni- $K\beta$ filter and zero-background plate holder. Phase analysis was performed using the PDF-2 database incorporated into PDXL program software.⁴⁰

IV. RESULTS AND DISCUSSION

A. AGA search for stable LiNiB and $\text{Li}_2\text{Ni}_3\text{B}$ phases

The AGA search starts from the equal-atomic LiNiB with unit cells containing 4, 6, 8, and 12 formula units. The energy for the low-energy structures of LiNiB with 4, 6, and 8 formula units obtained from our AGA search is shown as a function of the volume in Fig. 2. The lowest-energy structure has a $P2_1/c$ symmetry as shown in Fig. 3(a), and the crystallographic details of it are given in Table I. There is one Wyckoff site for each of Li, Ni, and B. This $P2_1/c$ LiNiB crystal structure was indeed confirmed experimentally recently.²³ The LiNiB ($P2_1/c$) with four formula units is noted as the RT-sg14 structure hereafter. We found that the RT-sg14 LiNiB obtained from our search could be viewed as a layered structure, which consists of alternate stacking of Li layer and Ni–B layer, as plotted in Figs. 3(b) and 3(c). The Li layer shows a close-packed motif with slightly different Li–Li bond distances along different directions, while in the Ni–B layer, B atoms form dimers and are surrounded by six Ni atoms. The coordination number for Li is 6 Li with an average distance of 2.93 \AA . Each Ni is surrounded by 3 Ni at an average distance of 2.48 \AA and 4 B at an average distance of 2.02 \AA . Boron form pairs with a B–B distance of 1.72 \AA . It is worth noting that all 23 low energy structures as shown in the red

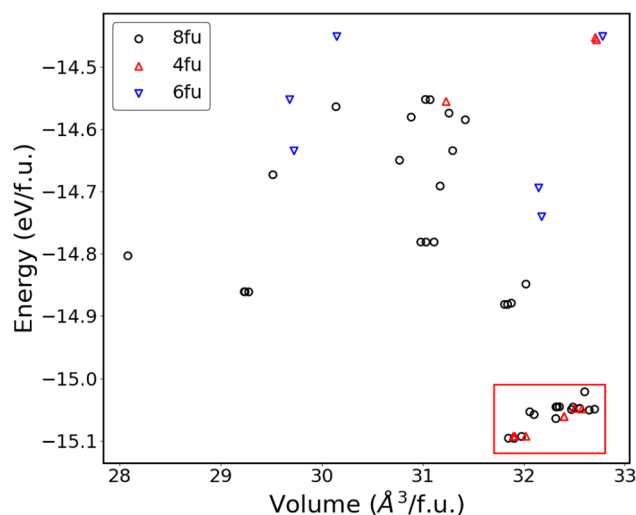


FIG. 2. Energy vs volume for the low-energy structures of LiNiB with 4, 6, and 8 f.u. per unit cell from the AGA search. The structures in red rectangle are 23 low-energy structures, and all of them have layered structure.

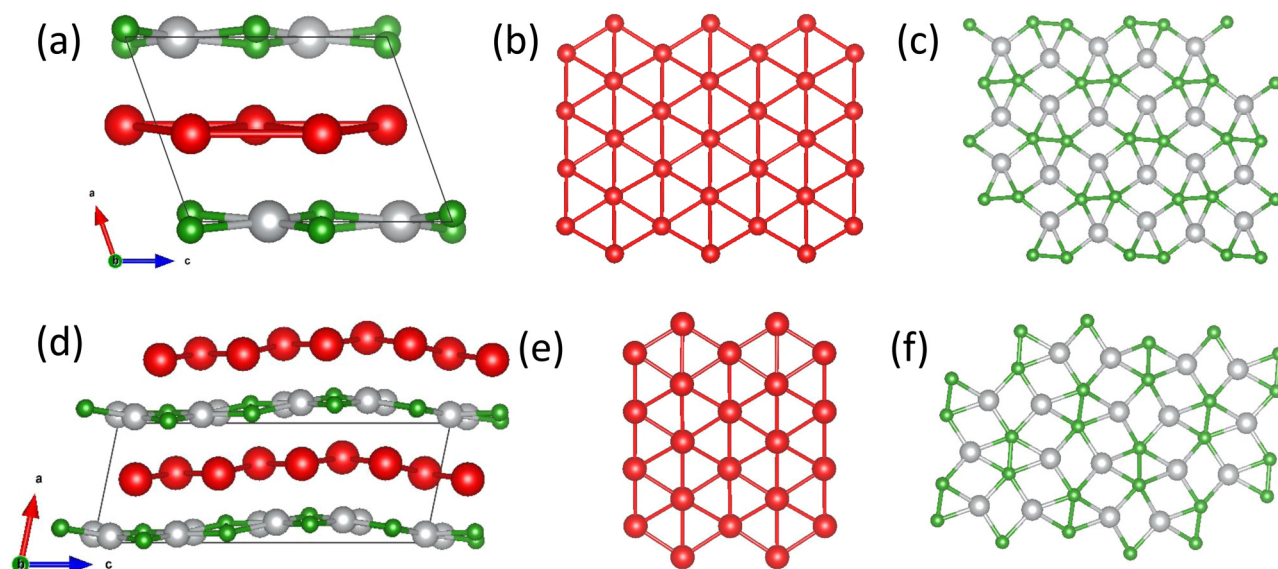


FIG. 3. The crystal structures of (a) RT-sg14 LiNiB with (b) Li layers and (c) NiB layers. (d) One of the distorted layer structures with (e) distorted Li layers and NiB layers (f). Li atoms are colored in red, Ni atoms are colored in gray, and B atoms are colored in green.

rectangle in Fig. 2 are layered structures, and three of them have distorted Li layers and NiB layers. One of distorted structure is shown in Figs. 3(d)–3(f). Calculations indicate an abundance of layered low-energy structures within a narrow energy range, suggesting that the real structure of LiNiB is an intergrowth of different stacking variants of [NiB] layers alternating with Li layers with additional variation within the layer. This is consistent with recent experimental findings.²³

Next, we extend the AGA search to a range of different components surrounding the LiNiB = 1:1:1 atomic ratio (i.e., 211, 121, 112, 311, 131, 113, 221, 122, 212, 321, 312, 123, 132, 231, 213, 141, and 341) with 4 and 6 formula units per unit cell. During the whole search process with different compositions, we used the following method to assess the stability of new compound. For any ternary compound $A_xB_yC_z$, its formation can be represented by the following chemical equation: $a^*A_{x1}B_{y1}C_{z1} + b^*A_{x2}B_{y2}C_{z2} + c^*A_{x3}B_{y3}C_{z3} \rightarrow A_xB_yC_z$, where $A_{x1}B_{y1}C_{z1}$, $A_{x2}B_{y2}C_{z2}$, and $A_{x3}B_{y3}C_{z3}$ can be any combination of known compounds that give non-negative values for a , b , and c . The formation energy E_F can then be calculated as: $E_F = E(A_xB_yC_z) - a^*E(A_{x1}B_{y1}C_{z1}) - b^*E(A_{x2}B_{y2}C_{z2}) - c^*E(A_{x3}B_{y3}C_{z3})$. If all possible values of E_F are less than zero, then we consider this compound to be energetically stable.

TABLE I. Crystallographic data of RT-sg14 LiNiB (space group $P2_1/c$, $Z = 4$).

Stable phase	Wyckoff site	Atom	x	y	z
LiNiB	4e	Li	0.024 11	0.744 55	0.379 82
	4e	Ni	0.498 14	0.499 62	0.200 17
	4e	B	0.456 24	0.325 92	0.489 01

These AGA searches result in a few new structures with energies very close to the existing convex hull as listed in the [supplementary material](#) Table S1. All experimental phases and our AGA searched phases, including the symmetry, lattice parameters, and formation energies above the convex hull, are listed in the [supplementary material](#) Table S1. Among them, a new Li_2Ni_3B phase, with four formula units $Z = 4$ and a space group of $P4_332$ (No. 212), is found to have energy even smaller than the Gibbs triangle formed by the existing stable phases on the ternary phase diagram. Therefore, the appearance of the Li_2Ni_3B changes the existing phase diagram dramatically.

As shown in Fig. 4(a), the crystal structure of the new phase Li_2Ni_3B can be represented as an interconnected network of distorted octahedra $Li@Li_3Ni_3$ and $B@Ni_6$. The average bond lengths of Li–Li, Li–Ni, and B–Ni are 2.448 Å, 2.507 Å, and 2.016 Å, respectively. The crystallographic details of the new Li_2Ni_3B structure are given in Table II. There is one Wyckoff site for each of Li (8c), Ni (12d), and B (4a). Upon close inspection, the new Li_2Ni_3B is found to be isostructural to two known compounds, Li_2Pd_3B and Li_2Pt_3B ⁴¹ ($P4_332$), which are stable phases in a cubic structure composed of distorted octahedral units of BPd_6 and BPt_6 . Note that the measurements of thermodynamic and transport properties revealed a superconducting transition temperature T_c of 7–8 K in Li_2Pd_3B and around 2.5 K in Li_2Pt_3B .^{42,43} T_c increases as the size and mass of the second element decreases⁴⁴ according to the Bardeen, Cooper, and Schrieffer (BCS)⁴⁵ microscopic theory of superconductivity. Since Ni, Pd, and Pt are isoelectronic elements, and Ni is lighter than Pd, we expect the isostructural Li_2Ni_3B to have a higher superconducting transition temperature than Li_2Pd_3B . Therefore, it would be interesting to synthesize $P4_332$ -type Li_2Ni_3B and measure its superconducting properties.

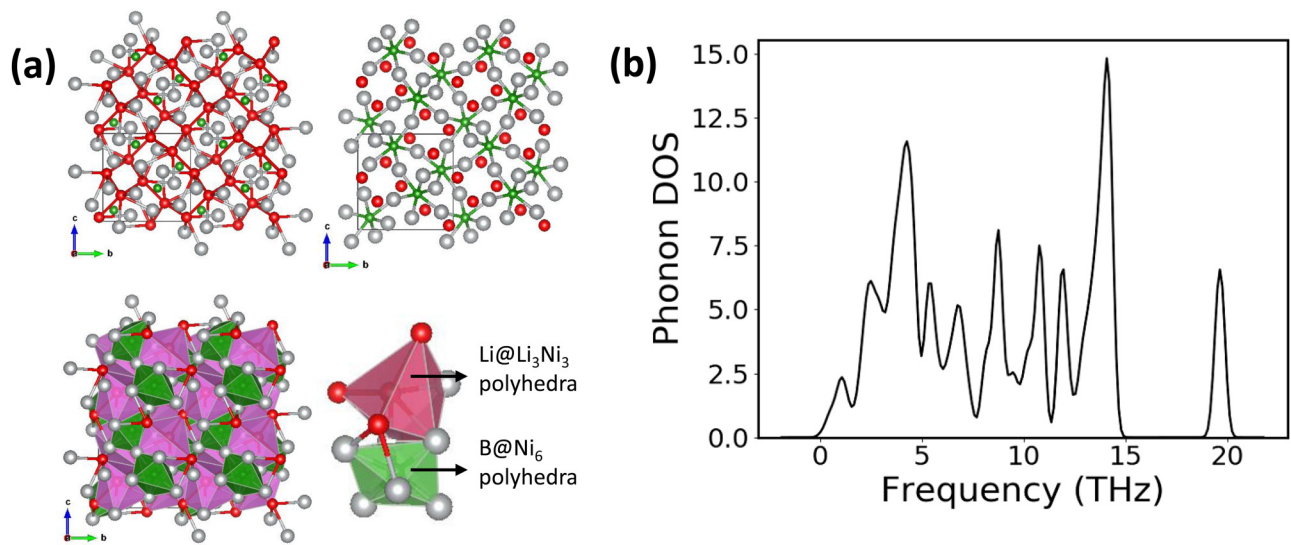


FIG. 4. (a) The configuration of $\text{Li}_2\text{Ni}_3\text{B}$ from AGA search. (b) Phonon density of states of $\text{Li}_2\text{Ni}_3\text{B}$.

To further investigate its dynamical stability, we performed phonon calculation for $\text{Li}_2\text{Ni}_3\text{B}$ using the density functional perturbation theory (DFPT) via the Phonopy code.⁴⁶ The phonon density of states (DOS) of the $\text{Li}_2\text{Ni}_3\text{B}$ phase is plotted in Fig. 4(b), showing that the $\text{Li}_2\text{Ni}_3\text{B}$ structure is dynamically stable without any soft phonon mode. To estimate the stability of $\text{Li}_2\text{Ni}_3\text{B}$ at elevated temperatures, we ran *ab initio* molecular dynamics (MD) simulations for 60 ps at temperatures of 300 K, 500 K, and 800 K, respectively. The energy curve is shown in the [supplementary material](#), Fig. S2, it can be seen that the structure can maintain stability.

It is worthwhile to discuss in more detail about a metastable ternary compound Li_2NiB in the space group of $Pmna$, whose formation energy is only 0.4 meV/atom above the hull. The crystallographic details of the new $\text{Li}_2\text{Ni}_3\text{B}$ structure are given in the [supplementary material](#), Table S2. As shown in Fig. 5, the $Pmna$ Li_2NiB is also a layered structure with the same Ni-B layer in RT-sg14 LiNiB , and the Li layer is also the same. The only difference is that there is one more Li layer in each unit cell of Li_2NiB . The formation energy of Li_2NiB , $E(\text{Li}_2\text{NiB}) \approx E(\text{LiNiB}) + E(\text{Li})$, thus, there is little extra cost in energy to insert an additional Li layer into the layered LiNiB structure. Remarkably, there is a family of layered orthorhombic transition metal borides with the general formula of $(\text{MB})_2\text{Al}_y(\text{MB}_2)_x$ (labeled as MAB phases, M can be Cr, Mo, W, Fe, Mn) that possess structural similarity to the $\text{Li}_x(\text{NiB})$

phases, i.e., the MB sublattice interleaved by one or two Al layers.^{47–49} Therefore, it is worth exploring whether the Li_2NiB structure really exists. In other words, can more than one Li layer be inserted between two NiB layers?

B. Electronic structure and electrochemical performance

Figure 6 shows the electronic density of states (DOS) and band structure along high symmetric lines of the Brillouin zone of the newly identified $\text{Li}_2\text{Ni}_3\text{B}$ compound and Li_2NiB . Both of them are found to be metallic with non-zero density of states at the Fermi level. For the band structure, Ni atomic orbitals, particularly Ni-3d, have the major contribution to the states right below the Fermi level.

We notice that the lowest energy structures of LiNiB and Li_2NiB are all layered structures. The intercalation voltage is an important parameter of lithium ion battery. In the ideal material, the voltage plateaus of the positive electrode material are high enough, and the voltage plateaus of the negative electrode material are low enough to obtain a higher working voltage, thereby providing a higher energy density of lithium ion battery. We calculated the voltage platform during the process of lithiation and delithiation to explore the electrochemical properties of the two layered

TABLE II. Crystallographic data of $\text{Li}_2\text{Ni}_3\text{B}$ (space group of $P4_332$, $Z = 4$).

Phase	Lattice parameter	Wyckoff site	Atom	x	y	z
$\text{Li}_2\text{Ni}_3\text{B}$	$a = b = c = 6.291$ $\alpha = \beta = \gamma = 90^\circ$	8c	Li	0.79405	0.79405	0.79405
		12d	Ni	0.12500	0.68377	0.56623
		4a	B	0.12500	0.12500	0.12500

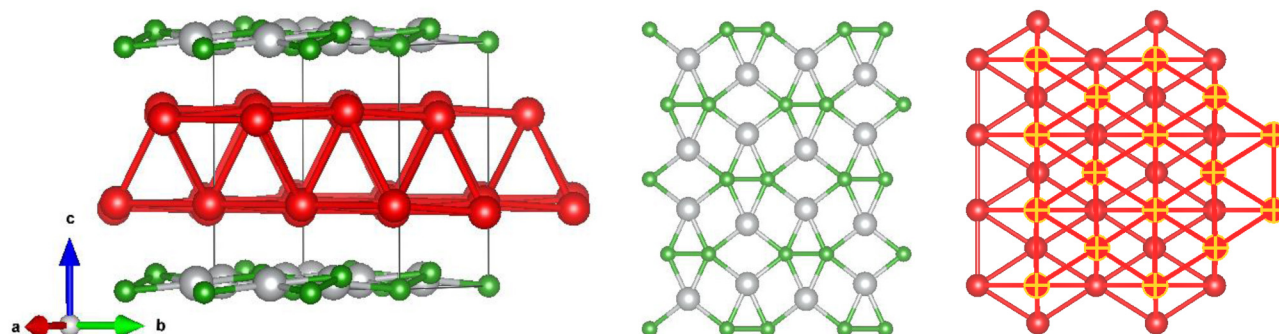


FIG. 5. The configuration of $Pmna$ Li_2NiB from AGA search. Li atoms are colored in red, Ni atoms are colored in gray, and B atoms are colored in green.

structures. The voltage is calculated with⁵⁰

$$V_{xy} = \frac{E_{\text{Li}_x\text{NiB}} - E_{\text{Li}_y\text{NiB}} - (x - y)E_{\text{Li}}}{x - y}, \quad (6)$$

where $E_{\text{Li}_x\text{NiB}}$ and $E_{\text{Li}_y\text{NiB}}$ are the energies of Li_xNiB and Li_yNiB , respectively, and E_{Li} is the energy of bulk Li. As shown in Fig. 7, there are no intermediate negative formation energy structures for LiNiB , so the voltage plateaus at 0.41 V. For Li_2NiB , there is one stable intermediate phase LiNiB , so the voltage plateaus at 0.58 V and 0.02 V. From the low values of the voltage plateau, it can be seen that these layered structures have a potential as anode materials for lithium ion batteries.

C. Construction of the Li-Ni-B ternary convex hull

With the discovered new compound, the existing convex hull of the Li-Ni-B system is updated in Fig. 8 to show the stability of

new and existing phases based on the DFT energies. In the current databases (i.e., Materials Project⁸ and Inorganic Crystal Structure Database²⁴), there are some reported binary and ternary phases (see Table S1 in the supplementary material). Among them, six binary phases LiB , LiB_3 , Li_3B_{14} , Ni_2B , Ni_3B , and Ni_4B_3 and three ternary phases, $\text{Li}_{1.2}\text{Ni}_{2.5}\text{B}_2$, $\text{Li}_3\text{Ni}_{20}\text{B}_6$, and $\text{Li}_{2.8}\text{Ni}_{16}\text{B}_8$ in hexagonal, cubic, and tetragonal crystal structures are energetically stable according to our DFT calculations. The Li_3B_{14} structure in a tetragonal cell (SG#81) was soundly stable from.⁵¹ Two ternary phases ($\text{LiNi}_3\text{B}_{1.8}$ and $\text{Li}_{2.8}\text{Ni}_{16}\text{B}_8$) were reinvestigated by Gvozdetzkyi *et al.*²² recently. The convex hull of the Li-Ni-B system has been updated with the inclusion of the new LiNiB phase obtained experimentally.²³

With a binary system, the compositional space is one-dimensional so that the convex hull is a curve that connects the formation energies of all adjacent stable phases. In a ternary system, the compositional space is combined by multiple regular triangular pieces as shown in Fig. 8. The convex hull is then composed of planes connecting the formation energies of all possible three stable

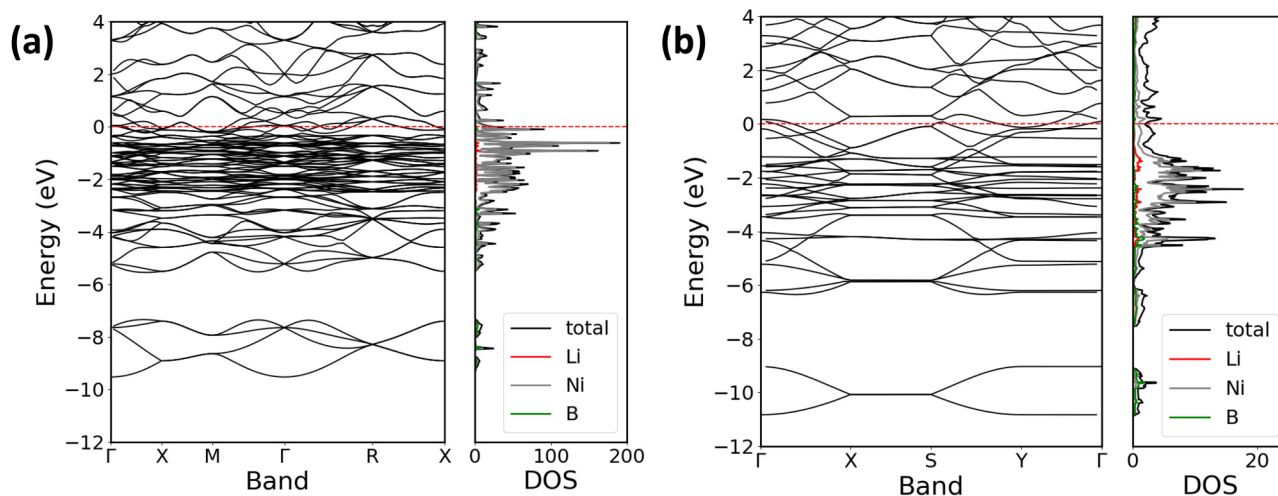


FIG. 6. Band and DOS diagrams of (a) $\text{Li}_2\text{Ni}_3\text{B}$ and (b) Li_2NiB . The zero energy is taken at the Fermi level. Atomic contributions into DOS are color coded: Li—red, Ni—grey, and B—green.

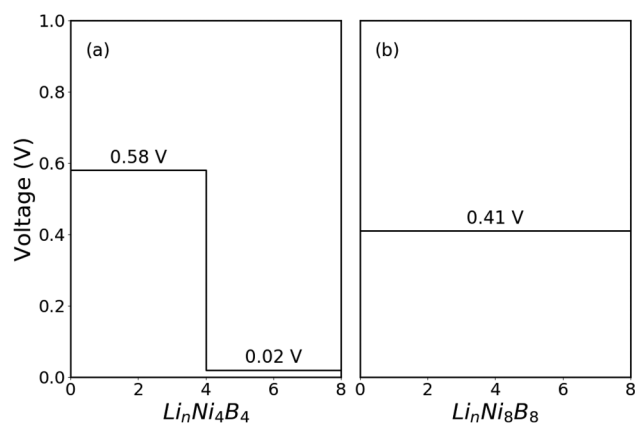


FIG. 7. Voltage variation of the two layer structures: (a) *Pmna* Li_2NiB and (b) *P2₁/c* LiNiB .

phases. The surface formed by the bottom pieces of planes at any composition is the convex hull surface. The formation energies of all known stable structures are located on the surface of this convex cladding. Any new structure having formation energy below this convex hull surface will be a new stable structure and the convex hull surface will be re-constructed by considering the formation energy of the newly discovered structure.

Energies of all the binary and ternary phases previously reported in the Li–Ni–B system were evaluated by GGA calculations and used to plot Fig. 8(a), where stable phases were represented by solid (red) triangles and metastable phases (i.e., with formation energies above the convex hull) were represented by hollow (blue) triangles. It can be seen that although reported by experiments, some phases such as NiB and $\text{Li}_3\text{Ni}_{16}\text{B}_8$, etc., are actually metastable at zero temperature according to our energy calculations.

The thermodynamic stability of $\text{Li}_2\text{Ni}_3\text{B}$ is determined by the Gibbs triangle formed by LiNiB , $\text{Li}_3\text{Ni}_{20}\text{B}_6$, and Li after considering the stable LiNiB phase as shown in Fig. 8(a): $\text{Li}_2\text{Ni}_3\text{B} \rightarrow (\text{Li}_3\text{Ni}_{20}\text{B}_6 + \text{LiNiB} + 10\text{Li})/7$. Our DFT calculations show that

the formation energy of left hand and right hand are -214.7 and -203.6 meV/atom, respectively. Negative formation energy occurs at the Li:Ni:B composition equal to 2:3:1 based on the new ternary convex hull after considering the stable LiNiB phase, indicating that the $\text{Li}_2\text{Ni}_3\text{B}$ compound is a new energetically stable phase. The calculated phase diagram of the Li–Ni–B system at 0 K can be updated in Fig. 8(b) with the inclusion of the new stable $\text{Li}_2\text{Ni}_3\text{B}$ phase.

We have repeated the DFT calculation by different DFT approximations, including GGA, local density approximation (LDA),⁵² GGA + U, and LDA + U. We recalculated all the stable phases (Li , Ni , LiB , LiB_3 , Li_3B_{14} , Ni_3B , Ni_2B , Ni_4B_3 , LiNiB , LiNi_3B_2 , $\text{Li}_3\text{Ni}_{20}\text{B}_6$, and $\text{Li}_2\text{Ni}_3\text{B}$) and two metastable phases (Li_2NiB and $\text{Li}_3\text{Ni}_{16}\text{B}_8$) that are very close to the convex-hull plane. A series of effective $U_{\text{eff}} = U - J = 1, 2, 3, 4$, and 5 eV are used for Ni atoms. As shown in the supplementary material, Table S3, Li , Ni , B , LiB , LiB_3 , Li_3B_{14} , Ni_3B , Ni_2B , Ni_4B_3 , LiNiB , LiNi_3B_2 , and $\text{Li}_3\text{Ni}_{20}\text{B}_6$ are always stable under different DFT approximations. However, the $\text{Li}_2\text{Ni}_3\text{B}$ phase is stable under GGA and GGA + U but is metastable under LDA and LDA + U. In contrast, the Li_2NiB and $\text{Li}_3\text{Ni}_{16}\text{B}_8$ phases are metastable under GGA and GGA + U but are stable under LDA and LDA + U. The LDA calculated phase diagram of the Li–Ni–B system at 0 K can be updated in the supplementary material, Fig. S1 with the inclusion of the stable Li_2NiB and $\text{Li}_3\text{Ni}_{16}\text{B}_8$ phases. While these new results do show that there is some uncertainty with DFT calculations, we believe that our results are still meaningful for guiding experiments because it is well known that a lot of experimental structures in various systems have formation energies above the Gibbs triangle of the convex-hull.

D. Experimental results

The hydride method of synthesis that was successfully utilized for the preparation of a predicted LiNiB compound²³ was utilized for search for another predicted here, $\text{Li}_2\text{Ni}_3\text{B}$ phase. Considering the fact that for synthesis of ternary compounds in Li–Ni–B systems, excess of Li is needed,^{19–23} two nominal loading compositions were examined: $\text{LiH:Ni:B} = 2:3:1$ and $3:3:1$ molar ratios. Analysis of the x-ray powder diffraction data indicated the presence

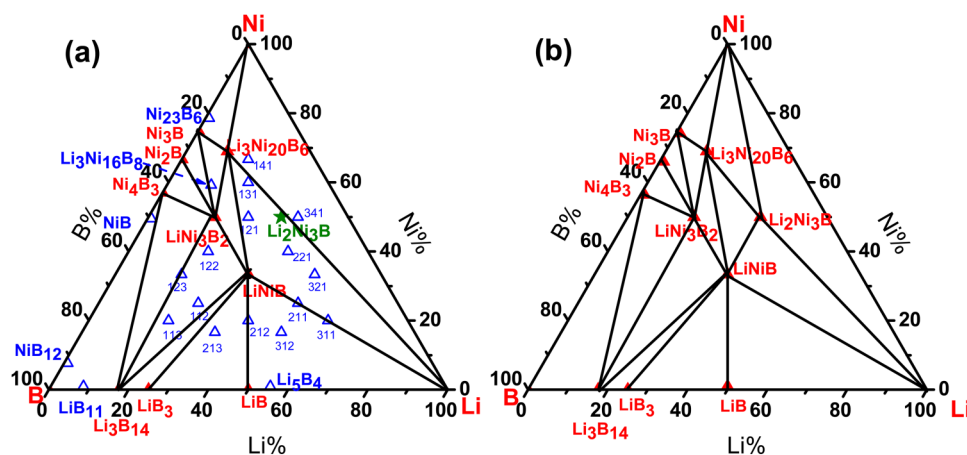


FIG. 8. Calculated convex hull of the formation energies in the Li–Ni–B system based on the previously reported phases (a) and after including the newly discovered $\text{Li}_2\text{Ni}_3\text{B}$ phase (b). All calculations were carried out at 0 K. Red solid triangles in the ternary phase diagram represent stable compounds, the green solid star represents a newly found stable phase, and blue hollow triangles indicate the metastable phases. The black lines separate the composition space into Gibbs triangles.

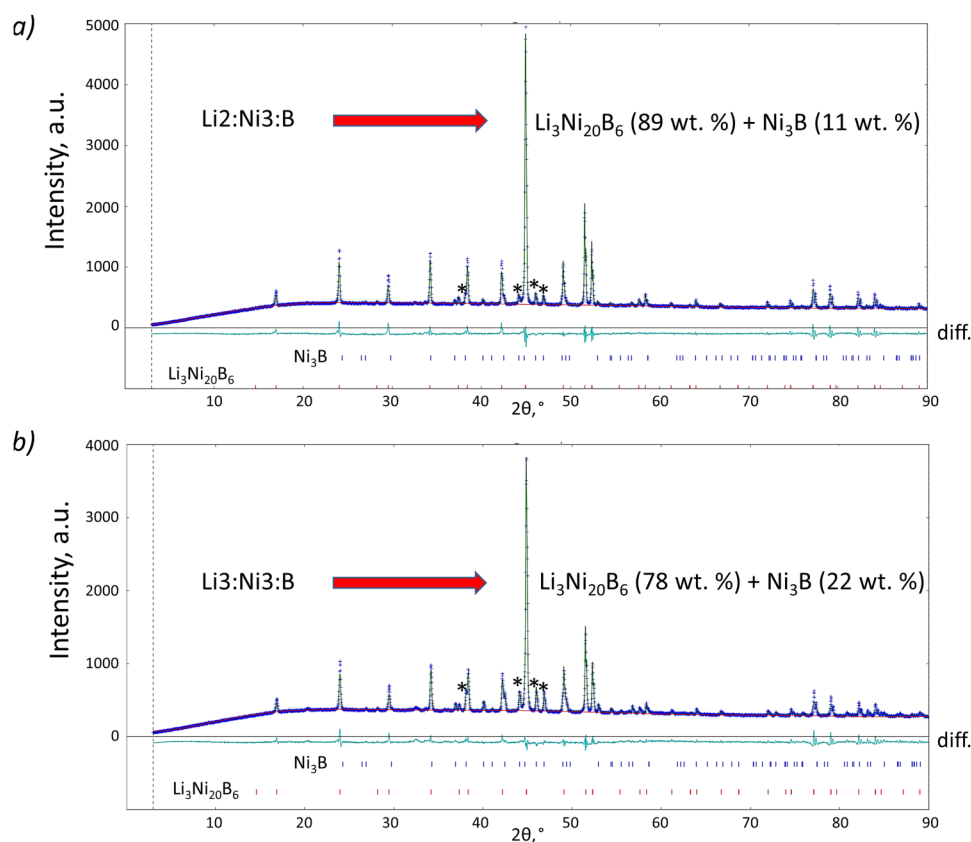


FIG. 9. Powder x-ray diffraction patterns of samples with nominal LiH:Ni:B = 2:3:1 (a) and 3:3:1 (b) molar ratios. $\text{Li}_3\text{Ni}_{20}\text{B}_6$ is the main product and the most intense peaks of Ni_3B are marked with *.

of $\text{Li}_3\text{Ni}_{20}\text{B}_6$ and Ni_3B phases only for two cases (89/11 wt. % and 78/22 wt. %, giving elemental overall compositions $\text{Li}_{0.40}\text{Ni}_3\text{B}_{0.91}$ and $\text{Li}_{0.35}\text{Ni}_3\text{B}_{0.92}$, respectively), with no additional peaks of potentially unknown compounds (Fig. 9). While calculated B content is only slightly underestimated (e.g., because of unreacted B in amorphous state), Li metal (considerably unreacted excess) was not observed from powder x-ray diffraction experiments due to the very small scattering factor (Li is light element). However, moving from the 2:3:1 to a 3:3:1 composition of the sample, we observed increased softness of the material in accordance with the increased content of the ductile Li metal.

V. CONCLUSION

In conclusion, we searched for possible thermodynamically stable Li–Ni–B crystal structures with different compositions using the adaptive genetic algorithm method and first-principles calculations based on density function theory. We successfully validated the layered structure of $P2_1/c$ LiNiB , which matches with the experimentally determined structure. The newly predicted cubic structure of $\text{Li}_2\text{Ni}_3\text{B}$ is energetically and dynamically stable based on GGA calculation, although this compound was not obtained experimentally. We believe that alternative synthesis methods other than hydride synthesis should be used for the

preparation of $\text{Li}_2\text{Ni}_3\text{B}$. Measurements of its superconducting properties are also desirable. The voltage platform during the process of lithiation and delithiation were calculated to explore the electrochemical properties of two layered structures, LiNiB and Li_2NiB . According to our electrochemical calculations, the two layered structures have the potential to be anode materials for lithium batteries. We updated the theoretical phase diagram of Li–Ni–B ternary phase based on the results of DFT calculations. The predictions from our theoretical studies provide useful guidance for experimental synthesis and discovery of new compounds for Li–Ni–B and similar systems.

SUUPPLEMENTARY MATERIAL

See the [supplementary material](#) for the details of the structure database of Li–Ni–B system, the crystallographic data of Li_2NiB , the difference of GGA and LDA, the convex-hull of LDA calculation, and the *ab initio* molecular dynamics (MD) simulations results. The following files are available free of charge.

ACKNOWLEDGMENTS

R. Wang acknowledges the support from the USTC and the China Scholarship Council (File No. 201906340034). The work at University of Science and Technology of China was supported by

the National Natural Science Foundation of China (NNSFC, Nos. 11574284 and 11774324) and the Supercomputing Center of USTC. The work at Ames Laboratory was supported by the U.S. Department of Energy (DOE), Basic Energy Sciences, Materials Science and Engineering Division, under Contract No. DEAC02-07CH11358, including a grant of computer time at the National Energy Research Scientific Computing Center (NERSC) in Berkeley, CA. Financial support for J.V.Z. start-up funds from the Iowa State University is gratefully acknowledged. L. Xu acknowledges the support from China Scholarship Council (File No. 201806310018).

REFERENCES

- ¹M. de Jong, W. Chen, T. Angsten, A. Jain, R. Notestine, A. Gamst, M. Sluiter, C. K. Ande, S. van der Zwaag, and J. J. Plata, *Sci. Data* **2**, 150009 (2013).
- ²K. Alberi, M. B. Nardelli, A. Zakutayev, L. Mitas, S. Curtarolo, A. Jain, M. Fornari, N. Marzari, I. Takeuchi, M. L. Green, M. Kanatzidis, M. F. Toney, S. Butenko, B. Meredig, S. Lany, U. Kattner, A. Davydov, E. S. Toberer, V. Stevanovic, A. Walsh, N.-G. Park, A. Aspuru-Guzik, D. P. Tabor, J. Nelson, J. Murphy, A. Setlur, J. Gregoire, H. Li, R. Xiao, A. Ludwig, L. W. Martin, A. M. Rappe, S.-H. Wei, and J. Perkins, *J. Phys. D Appl. Phys.* **52**, 013001 (2018).
- ³J. Pannetier, J. Bassas-Alsina, J. Rodriguez-Carvajal, and V. Caignaert, *Nature* **346**, 343 (1990).
- ⁴C. J. Pickard and R. J. Needs, *J. Phys. Condens. Matter* **23**, 053201 (2011).
- ⁵A. R. Oganov and C. W. Glass, *J. Chem. Phys.* **124**, 244704 (2006).
- ⁶Y. Wang, J. Lv, L. Zhu, and Y. Ma, *Phys. Rev. B* **82**, 094116 (2010).
- ⁷Y. Wang, J. Lv, L. Zhu, and Y. Ma, *Comput. Phys. Commun.* **183**, 2063 (2012).
- ⁸A. Jain, S. P. Ong, G. Hautier, W. Chen, W. D. Richards, S. Dacek, S. Cholia, D. Gunter, D. Skinner, G. Ceder, and K. A. Persson, *APL Mater.* **1**, 011002 (2013).
- ⁹J. E. Saal, S. Kirklin, M. Aykol, B. Meredig, and C. Wolverton, *JOM* **65**, 1501 (2013).
- ¹⁰See <https://cmr.fysik.dtu.dk/> for information about computational materials.
- ¹¹S. Curtarolo, W. Setyawan, S. Wang, J. Xue, K. Yang, R. H. Taylor, L. J. Nelson, G. L. W. Hart, S. Sanvito, M. Buongiorno-Nardelli, N. Mingo, and O. Levy, *Comput. Mater. Sci.* **58**, 227 (2012).
- ¹²See <http://gurka.fysik.uu.se/ESP/> for information about electronic structure of materials.
- ¹³G. Akopov, M. T. Yeung, and R. B. Kaner, *Adv. Mater.* **29**, 1604506 (2017).
- ¹⁴J. F. Herbst, J. J. Croat, F. E. Pinkerton, and W. Yelon, *Phys. Rev. B* **29**, 4176 (1984).
- ¹⁵X. Tan, P. Chai, C. M. Thompson, and M. Shatruk, *J. Am. Chem. Soc.* **135**, 9553 (2013).
- ¹⁶J. Nagamatsu, N. Nakagawa, T. Muranaka, Y. Zenitani, and J. Akimitsu, *Nature* **410**, 63 (2001).
- ¹⁷H. Park, A. Encinas, J. P. Scheifers, Y. Zhang, and B. P. Fokwa, *Angew. Chem. Int. Ed.* **56**, 5575 (2017).
- ¹⁸M. T. Yeung, R. Mohammadi, and R. B. Kaner, *Annu. Rev. Mater. Res.* **46**, 465 (2016).
- ¹⁹W. Jung, *Z. für Kristallogr.-Cryst. Mater.* **151**, 113 (1980).
- ²⁰W. Jung, *Naturwissenschaften* **63**, 246 (1976).
- ²¹W. Jung, *Z. für Naturforsch. B* **32**, 1371 (1977).
- ²²V. Gvozdetzkyi, M. P. Hanrahan, R. A. Ribeiro, T. H. Kim, L. Zhou, A. J. Rossini, P. C. Canfield, and J. V. Zaikina, *Chem. -Eur. J.* **25**, 4123 (2019).
- ²³V. Gvozdetzkyi, G. Bhaskar, M. Batuk, X. Zhao, R. Wang, S. L. Carnahan, M. P. Hanrahan, R. A. Ribeiro, P. C. Canfield, A. J. Rossini, C.-Z. Wang, K.-M. Ho, J. Hadernmann, and J. V. Zaikina, *Angew. Chem., Int. Ed.* **58**, 15855 (2019).
- ²⁴See <https://icsd.fiz-karlsruhe.de/> for information about experimental structures (2019).
- ²⁵X. Zhao, M. C. Nguyen, W. Y. Zhang, C. Z. Wang, M. J. Kramer, D. J. Sellmyer, X. Z. Li, F. Zhang, L. Q. Ke, V. P. Antropov, and K. M. Ho, *Phys. Rev. Lett.* **112**, 045502 (2014).
- ²⁶Z. Ye, F. Zhang, Y. Sun, M. C. Nguyen, S. H. Zhou, L. Zhou, F. Meng, R. T. Ott, E. Park, M. F. Besser, M. J. Kramer, Z. J. Ding, M. I. Mendelev, C. Z. Wang, R. E. Napolitano, and K. M. Ho, *Phys. Rev. Mater.* **1**, 055601 (2017).
- ²⁷R. Wang, Y. Sun, V. Antropov, Z. Lin, C.-Z. Wang, and K.-M. Ho, *Appl. Phys. Lett.* **115**, 182601 (2019).
- ²⁸S. Q. Wu, M. Ji, C.-Z. Wang, M. C. Nguyen, X. Zhao, K. Umamoto, R. M. Wentzcovitch, and K.-M. Ho, *J. Phys.: Condens. Matter* **26**, 035402 (2014).
- ²⁹D. M. Deaven and K.-M. Ho, *Phys. Rev. Lett.* **75**, 288 (1995).
- ³⁰S. M. Foiles, M. I. Baskes, and M. S. Daw, *Phys. Rev. B* **33**, 7983 (1986).
- ³¹X. W. Zhou, R. A. Johnson, and H. N. G. Wadley, *Phys. Rev. B* **69**, 144113 (2004).
- ³²A. Banerjee and J. R. Smith, *Phys. Rev. B* **37**, 6632 (1988).
- ³³P. Brommer and F. Gähler, *Modell. Simul. Mater. Sci. Eng.* **15**, 295 (2007).
- ³⁴P. Brommer and F. Gähler, *Philos. Mag.* **86**, 753 (2006).
- ³⁵P. E. Blochl, *Phys. Rev. B* **50**, 17953 (1994).
- ³⁶G. Kresse and J. Furthmüller, *Comput. Mater. Sci.* **6**, 15 (1996).
- ³⁷G. Kresse and J. Furthmüller, *Phys. Rev. B* **54**, 11169 (1996).
- ³⁸J. P. Perdew, K. Burke, and M. Ernzerhof, *Phys. Rev. Lett.* **77**, 3865 (1996).
- ³⁹H. J. Monkhorst and J. D. Pack, *Phys. Rev. B* **13**, 5188 (1976).
- ⁴⁰PDXL: Integrated X-ray powder diffraction software, Version 2.8.1.1. Rigaku, (2018).
- ⁴¹U. Eibenstein and W. Jung, *J. Solid State Chem.* **133**, 21 (1997).
- ⁴²K. Togano, P. Badica, Y. Nakamori, S. Orimo, H. Takeya, and K. Hirata, *Phys. Rev. Lett.* **93**, 247004 (2004).
- ⁴³P. Badica, T. Kondo, and K. Togano, *J. Phys. Soc. Jpn.* **74**, 1014 (2005).
- ⁴⁴D. Welch, *Advances in Cryogenic Engineering Materials* (Springer, 1984), p. 671.
- ⁴⁵J. Bardeen, L. N. Cooper, and J. R. Schrieffer, *Physical Review* **108**, 1175 (1957).
- ⁴⁶A. Togo and I. Tanaka, *Scr. Mater.* **108**, 1 (2015).
- ⁴⁷M. Ade and H. Hillebrecht, *Inorg. Chem.* **54**, 6122 (2015).
- ⁴⁸S. Kota, E. Zapata-Solvas, A. Ly, J. Lu, O. Elkassabany, A. Huon, W. E. Lee, L. Hultman, S. J. May, and M. W. Barsoum, *Sci. Rep.* **6**, 26475 (2016).
- ⁴⁹J. Lu, S. Kota, M. W. Barsoum, and L. Hultman, *Mater. Res. Lett.* **5**, 235 (2017).
- ⁵⁰M. K. Aydinol, A. F. Kohan, G. Ceder, K. Cho, and J. Joannopoulos, *Phys. Rev. B* **56**, 1354 (1997).
- ⁵¹A. G. Van Der Geest and A. G. Kolmogorov, *Calphad* **46**, 184 (2014).
- ⁵²J. P. Perdew and A. Zunger, *Phys. Rev. B* **23**, 5048 (1981).